Macromolecules

Article

pubs.acs.org/Macromolecules

Reversible Fluorescence Switching of Spiropyran-Conjugated Biodegradable Nanoparticles for Super-Resolution Fluorescence Imaging

Ming-Qiang Zhu,*[,†] Guo-Feng Zhang,[†,§] Zhe Hu,[†,§] Matthew P. Aldred,[†] Chong Li,[†] Wen-Liang Gong,[†] Tao Chen,[†] Zhen-Li Huang,*[,†] and Shiyong Liu*[,‡]

[†]Wuhan National Laboratory for Optoelectronics, Huazhong University of Science and Technology, Wuhan, Hubei 430074, China

[‡]CAS Key Laboratory of Soft Matter Chemistry, Department of Polymer Science and Engineering, University of Science and Technology of China, Hefei, Anhui 230026, China

Supporting Information

ABSTRACT: We report on the reversible fluorescence switching of biodegradable nanoparticles of spiropyran-terminated poly(ε-caprolactone) (SP-PCL) for super-resolution fluorescence imaging. SP-PCL was synthesized via ring-opening polymerization using hydroxyl-containing SP derivative as the initiator. SP-PCL solution in THF or dioxane exhibits fast photochromism from colorless to blue upon UV irradiation due to the transformation of SPs in SP-PCL into merocyanines (MCs). Although both SP-PCL solution and MC-PCL solution do not fluoresce, SP-PCL nanoparticle dispersion fabricated via nanoprecipitation in aqueous media, in which SP molecules were embedded into the hydrophobic PCL matrix, displays considerable green emission at 530 nm at an excitation wavelength of 420 nm. Upon <420 nm irradiation, the resulting MC-PCL nanoparticles show strong red emission at 650 nm when excited at 420 nm. SP-PCL nanoparticles display green−red dual-color intrinsic fluorescence switching upon alternated UV/vis illumination. Green emission from SP in SP-PCL nanoparticles is observed before UV irradiation while red emission from MCs in MC-PCL nanoparticles after UV irradiation. For both SP-PCL and MC-PCL nanoparticles, the critical excitation wavelength is determined at 420 nm, at which the photoinduced interconversion of MC- and SP-forms are found to be at equilibrium. Positive and inverse photoisomerizations monitored using time-dependent fluorescence spectra show that blue light excitation above 420 nm yields green emission of SPs in SP-PCL nanoparticles while light irradiation below 420 nm imparts photoisomerization (SP to MC) and thus red emission of MCs in MC-PCL nanoparticles. Green and red fluorescence can be optically switched and imaged under fluorescent microscopy. Biodegradable SP-PCL nanoparticles are demonstrated to be promising photoswitchable fluorophores for localization-based super-resolution microscopy, evidencing by resolving nanostructures with sub-50 nm resolution in poly(vinyl alcohol) (PVA) film and live cells.

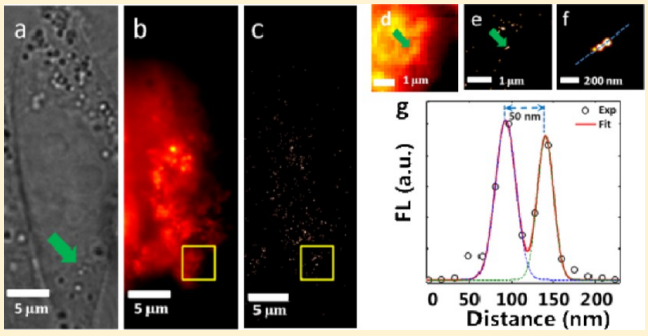

INTRODUCTION

During the past several decades, a great deal of intensive investigation has been devoted to photochromic materials[1−3] because they have high potential for applications, such as optically rewritable data storage,[4] optical switching,[5,6] and chemical sensing.[7] The photochromic or photoswitchable materials with higher sensitivity, higher speed, and less fatigue to stimuli are highly desirable. The effort on high performance of photoswitchable materials involves two stages, i.e., the development of novel molecular photoswitches as well as the integration of popular photoswitchable molecules into significant devices. The development of molecular photoswitches in the first stage is attributed to organic synthetic chemists while in the past decade most of researchers focus on the latter stage, that is, reinvestigation of current popular molecular photoswitches such as spiropyrans (SPs).[8−10] It is known that SP-based molecular switches exhibit dramatically different optical properties in different medium, i.e., free solution vs solid film. In the solid phase, the SP-based molecular switches exhibit much stronger fluorescence than solution and high resistance to fatiguing effect. Most of the studies reported to date are devoted to photoswitching carried out in bulk, or at least homogeneous media, whereas nanoparticles remain the basic building blocks of choice, which can be addressed individually for many fluorescent bioimaging applications.[11−13] Photoswitchable nanoparticles integrate two advantages of both solid and solution phases: fluorophores entangled in the nanoparticles like in the solid state and nanoparticles dispersible in solution for convenient manipulation, respectively.[12]

Received: January 15, 2014
Revised: February 11, 2014

   dx.doi.org/10.1021/ma5001157 | *Macromolecules* XXXX, XXX, XXX−XXX

Super-resolution imaging based on the nanoscale localization of photoswitchable fluorophores allows for capture of the images with a higher resolution than the diffraction limit, thus enabling *real-time* and *in situ* observation of the spatially complex and subcellular fine structures that cannot be resolved in conventional fluorescence microscopy.[14−21] Recent development of super-resolution fluorescence microscopy has substantively initiated the urgent aspiration toward exploration of novel types of photoswitchable probes.[22−24] As the essential prerequisite, however, current photoswitchable fluorescent materials are far from satisfactory. For instance, though the photoswitchable SP-containing nanoparticles that we prepared via emulsion polymerization offer the possibility to super-resolution imaging,[12] difficult degradation of these vinyl-based polymer nanoparticles under biological conditions prevents their practical applications in biology. Therefore, biodegradable photoswitchable fluorophores are highly desirable in order to extend localization-based super-resolution microscopy into the field of tissue or small animal imaging. There are reports about biocompatible nanoassembles with encapsulated noncovalently binding photoswitches while their fluorescence switching is relatively complicated.[25,26] Herein, we synthesize SP-containing biodegradable poly(ε-caprolactone) (PCL) polymer nanoparticles (SP-PCL) and investigate their photochromic and fluorescence photoswitching behaviors in the nanoscale condensed phase. Impressively, these SP-PCL nanoparticles exhibit the superior capabilities in distinguishing the subwavelength nanostructures and living cells by localization-based super-resolution microscopy.

EXPERIMENTAL SECTION

Materials. All commercially available starting materials, reagents, and solvents were used as supplied, unless otherwise stated. Isopropyl titanate (iPT, Sigma-Aldrich) was used as received without further purification. ε-Caprolactone (ε-CL) (Sigma-Aldrich) was purified by drying over calcium hydride (CaH_2) and distilling under reduced pressure. Calcium hydride, anhydrous ether, acetonitrile, dichloromethane, toluene, dioxane, and tetrahydrofuran (THF) were purchased from Sinopharm Chemical Reagent Co. Ltd., China. Dioxane, toluene, and THF were dried using sodium wire and benzophenone as indicator.

Synthesis of 2-(3′,3′-Dimethyl-6-nitrospiro[chromene-2,2′-indolin]-1′-yl)ethanol (SP-OH). SP-OH was prepared according to the previous literature[27] with slight modifications. The mixture of 2,3,3-trimethyl-3*H*-indole (16.06 g, 100.86 mmol) and 2-bromoethanol (13.23 g, 105.87 mmol) in acetonitrile (20 mL) was heated to reflux for 24 h under N_2. After cooling down to room temperature, the precipitation was filtered, washed with dichloromethane (DCM, 20 mL × 3), collected, and dried in the oven to afford **1** (26.33 g, yield 91.87%), which was used in next step without purification. A solution of **1** (6.02 g, 21.82 mmol) and KOH (2.78 g, 49.64 mmol) in distilled water (40 mL) was stirred at room temperature for 30 min and then was extracted with Et_2O (30 mL × 3). The organic layer was collected, dried with Na_2SO_4, and concentrated under reduced pressure to afford yellow oil. To the oil, a solution of 5-nitrososalicylaldehyde (4.21 g, 25.2 mmol) in ethanol (40 mL) was added, and the mixture was heated for 3 h to reflux under N_2. After cooling to room temperature, the precipitation was filtered, washed with ethanol, and dried to afford SP-OH as a purple solid (6.87 g, yield 89.34%). ^{1}H NMR (400 MHz, $CDCl_3$): 1.21 (s, 3H), 1.31 (s, 3H), 3.32−3.38 (m, 1H), 3.44−3.51 (m, 1H), 3.71−3.85 (m, 2H), 5.88 (d, 1H, J = 10.4 Hz), 6.67 (d, 1H, J = 8.0 Hz), 6.76 (d, 1H, J = 8.8 Hz), 6.90 (m, 2H), 7.10 (d, 1H, J = 7.6 Hz), 7.19 (t, 1H), 8.00 (m, 2H). MS m/z (APCI): $[M + 1]^+$: 353.0.

Preparation of SP-PCL. SP-PCL polymers were synthesized according to previous literature reports[28,29] with slight modifications. Typically, a solution of SP-OH (18 mg, 0.05 mmol) and isopropyl titanate (0.0125 mmol) in toluene was heated at 60 °C for 1 h under N_2, and then the resulting solvent was slowly removed in vacuum to obtain the SP initiators. Immediately, ε-caprolactone (2.2 mL, 20 mmol) was injected to the SP initiators via syringe. After the solution was heated at 80 °C and stirred for 10 h, the crude product was dissolved with chloroform and precipitated in methanol and then dried in the oven overnight at room temperature. The finally obtained SP-PCL polymers were analyzed for ^{1}H NMR and GPC. Gel permeation chromatography (GPC) indicates this particular copolymer to have a number-average molecular weight (M_n) of 32 900 with a polydispersity index (PDI) of 1.46.

Preparation of SP-PCL Nanoparticles. The solution of SP-PCL (10 mg) in dioxane (5 mL) was added to deionized water (45 mL) dropwise, and the SP-PCL dispersion obtained was dialyzed against deionized for 7 days with water exchange every 6 h to remove the organic solvent. The samples were dissolved in H_2O, filtered through syringe filter (Pall Corp., 0.22 μm), and stored. For SEM images, samples was dropped on the silicon chip and dried in the oven at room temperature for 48 h. SEM images were recorded with a Quamta 200 on silicon chip.

Delivery of the SP-PCL Nanoparticles into Live Cells. Briefly, 10 pmol of SP-PCL nanoparticles and 2 μL of Lipofectamine TM2000 (Invitrogen) in 50 μL of Opti-MEM I medium (Invitrogen) were mixed for 20 min at room temperature. Then the mixture was added to the well and incubated with the cells at 37 °C in 5% CO_2 incubator for 4 h. As a control, Lipofectamine TM2000 was intentionally not used to help deliver the SP-PCL nannoparticles into live cells. Before imaging, cells were washed three times with PBS buffer (pH = 7.4).

Super-Resolution Fluorescent Imaging. The optical setup for imaging was based on a home-built microscope setup consisted of an Olympus IX71 inverted optical microscope, a 100×/NA1.49 oil immersion TIRF objective (UAPON 100XOTIRF, Olympus), three solid-state lasers (405, 473, and 561 nm, all from CNILaser, China), and an Andor iXon 897 EMCCD camera. During super-resolution imaging, two electronic shutters (UNIBLITZ VS14, Vincent Associates) were used to control the duration of laser irradiance, and a dichroic mirror (Di01-R488/561, Semrock) and a long pass filter (BLP01-561R-25, Semrock) were used to separate the collected fluorescence from scattering laser and impurity fluorescence. The ImageJ plugins written in Java was used to analyze the images. An ultrafast and high-precision image analysis method, termed MaLiang (maximum likelihood algorithm encoded on a Graphics Processing Unit (GPU)), was established.[30,31] Briefly, Gaussian fitting with the following equation was used to localize the single molecules in the conventional fluorescence microscopy images.

$$I = I_{sig} \exp\left(-\frac{(i - x_0)^2 + (j - y_0)^2}{2s^2}\right) + I_{bkg}$$

Here (x_0, y_0) was the position of fluorescent molecule, s was the width of Gaussian kernel, and I_{sig} and I_{bkg} denoted the peak value of signal and the intensity of background photon (including background fluorescence, remnant laser scattering, and average readout noise), respectively. The localization precision for individual fluorescent molecule imaged by EMCCD camera could be calculated by

$$\langle \Delta x^2 \rangle = \frac{2s^2 + a^2/12}{\phi N} + \frac{16\pi s^4 (\phi I_b)}{a^2 (\phi N)^2}$$

where s is the width of Gaussian kernel, a is the pixel size, I_b is the background photon ($I_b = I_{bkg} - N_r^2$), N_r is the readout noise, Φ is the quantum efficiency, and N is the number of the photons collected.

In order to obtain super-resolution images, we utilized the green−red emission transition of the SP-PCL polymer nanoparticles. According to previous photophysical measurements, the red emission from the nanoparticles was significantly brighter than the green. On the other hand, autofluorescence might disturb the detection in green channel. Taking these aspects into consideration, we used the MC form of the SP-PCL nanoparticles for super-resolution imaging.

dx.doi.org/10.1021/ma5001157 | *Macromolecules* XXXX, XXX, XXX−XXX

Scheme 1. Preparation of SP-PCL Polymer

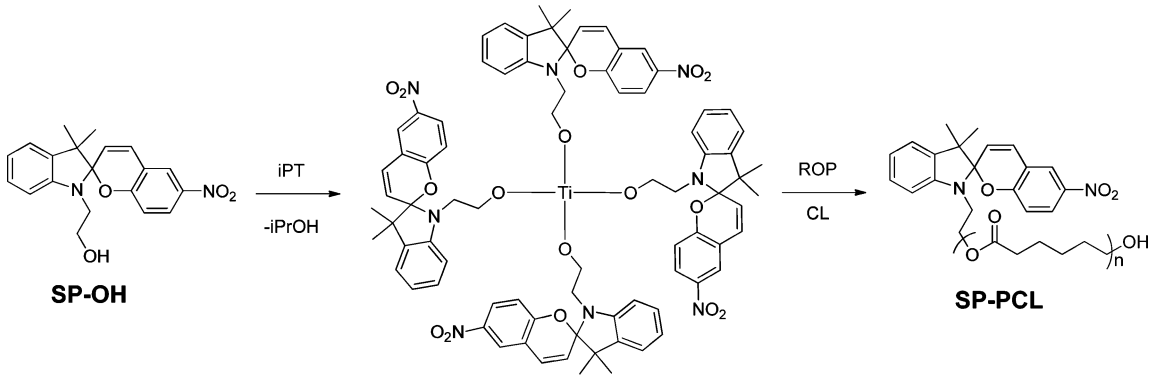

When the density of active MC-form nanoparticles was too low during the imaging, a weak 405 nm laser was flashed to convert the SP-form nanoparticles into MC-form ones. Repeating this cycle many times allowed us to achieve enough images for further super-resolution image reconstruction.

Characterization. ^{1}H NMR spectra are reported in parts per million (ppm) relative to tetramethylsilane as an internal standard. Gel permeation chromatography (GPC) (PL50 apparatus equipped with two PLgel 5 μm MIXED-C columns, 300 × 7.5 mm and one PL gel 5 μm Guard column, 50 × 7.5 mm) at 40. Tetrahydrofuran was served as eluent at flow rate of 1.0 mL/min. Polystyrene standard was used for calibration. H_2O (18.2 MΩ cm^{-1}) was purified with a Millipore Integral 3 system. UV absorbance spectra of SP-PCL polymer and nanoparticles were recorded with an UV-3600 UV−vis−NIR spectrophotometer (Shimadzu) at a wavelength scan rate of 4 nm/s. The absorbance change from photochromism of SP-PCL nanoparticles into MC-PCL nanoparticles were obtained after subtraction of the absorbance spectra between final MC-PCL nanoparticles and original SP-PCL nanoparticles. Fluorescence spectra of SP-PCL polymer and nanoparticles were recorded with a FLS 920 spectrophotometer (Edinburg) at a wavelength scan rate of ∼2 nm/s. The emission intensity change from photochromism of SP-PCL nanoparticles into MC-PCL nanoparticles were obtained upon continuous irradiation (excitation) at 400 nm. The crystallinity of the SP-PCL polymer at room temperature was measured by X-ray diffraction (XRD) and differential scanning calorimetry (DSC). DSC experiments were conducted from −50 to 100 °C at a heating rate of 10 °C/min under a nitrogen atmosphere. For XRD, the samples were placed in a quartz sample holder and scanned from 5° to 85° at a scanning rate of 5°/min. SP-PCL samples were prepared from a 90% water−dioxane solvent mixture and drop-casted onto glass slides, and the solvent was evaporated. Fluorescence microscopy is performed with a home-built TIRF microscope setup consisting of an Olympus IX 71 inverted microscope, a 100×/NA 1.49 oil immersion TIRF objective (UAPON 100XOTIRF, Olympus), a 405 nm laser diode and a 561 nm diode-pumped solid-state laser (both from CNILaser, China), and an Andor iXon 897 EMCCD camera.

RESULTS AND DISCUSSION

Synthesis of SP-PCL and Fabrication of SP-PCL Nanoparticles. SP-PCL was prepared via ring-opening polymerization of ϵ-caprolactone (CL) using SP-functionalized titanate as initiator (Scheme 1). The SP-functionalized titanate initiator was synthesized via transesterification between SP-OH and isopropyl titanate (iPT). The produced isopropanol was removed together with toluene overnight in reduced pressure. The CL monomer was injected to dissolve the initiator to obtain a brown solution. The polymerization was conducted at 80 °C for 10 h. The reaction mixture was dissolved in $CHCl_3$ and precipitated in methanol for three times to get a brown powder with 82% yield. The GPC measurement indicated that SP-PCL molecular weight and molecular weight distribution were 32 900 and 1.46, respectively. The ^{1}H NMR spectrum of SP-PCL is shown in Figure 1.

The preparation and photoswitching of SP-PCL polymer nanoparticles are shown in Scheme 2. SP-PCL self-assembled into nanoparticles with hydrophobic cores and hydrophilic surfaces to minimize the surface energy when dispersed in water. The bluish transparent nanoparticle dispersion is stable for at least one month, probably due to presence of hydrophilic terminal hydroxyl groups at the surface of polymer nanoparticles. Scanning transmission microscopic (SEM) imaging displays that as-prepared SP-PCL nanoparticles are nearly spherical with a narrow diameter distribution with sizes of 74.6 ± 9.3 nm (Figure 2a,b), and dynamic light scattering (DLS) measurement also confirms that SP-PCL nanoparticles in water possess rather uniform sizes (Figure 2c). We also notice that the average hydrated sizes of SP-PCL nanoparticles measured by DLS are about 80 nm, which is reasonably larger than that observed by SEM imaging.

Photochromism and Fluorescence Switching of SP-PCL Nanoparticles. The photochromic properties of SP-PCL depend on the solvents and dispersed states. As shown in Figure 3a, UV-induced maximum absorption wavelength of SP-PCL in toluene, dioxane, and THF shows a blue-shift, which is 605, 595, and 590 nm, respectively. The maximum absorption wavelength of SP-PCL in THF/water mixture even shifts to 558 nm. After exposure to UV irradiation at 365 nm for 5 s, the color of SP-PCL nanoparticle dispersion quickly changes to purple, accompanied by the appearance of an absorption band at 558 nm (Figure 3b).

Incorporation of SPs into the hydrophobic core of SP-PCL nanoparticles could give rise to improved on- and off-state fluorescence characteristics with extreme sensitivity toward light. Our previous studies showed that the merocyanine (MC) form of the molecular switches incorporated into the hydrophobic core of polymer nanoparticles was highly luminescent, whereas their SP form was almost nonfluorescent.[12] Compared with the previous investigation, there are both similarity and difference for the photoswitchable fluorescence property of as-synthesized SP-PCL nanoparticles. After UV light irradiation at 365 nm, the SPs inside the nanoparticle cores are switched to the MC form, and the fluorescence of the nanoparticles appears strong in the red region at 650 nm. However, it is out of our anticipation that, upon 420 nm excitation, a green

dx.doi.org/10.1021/ma5001157 | Macromolecules XXXX, XXX, XXX−XXX

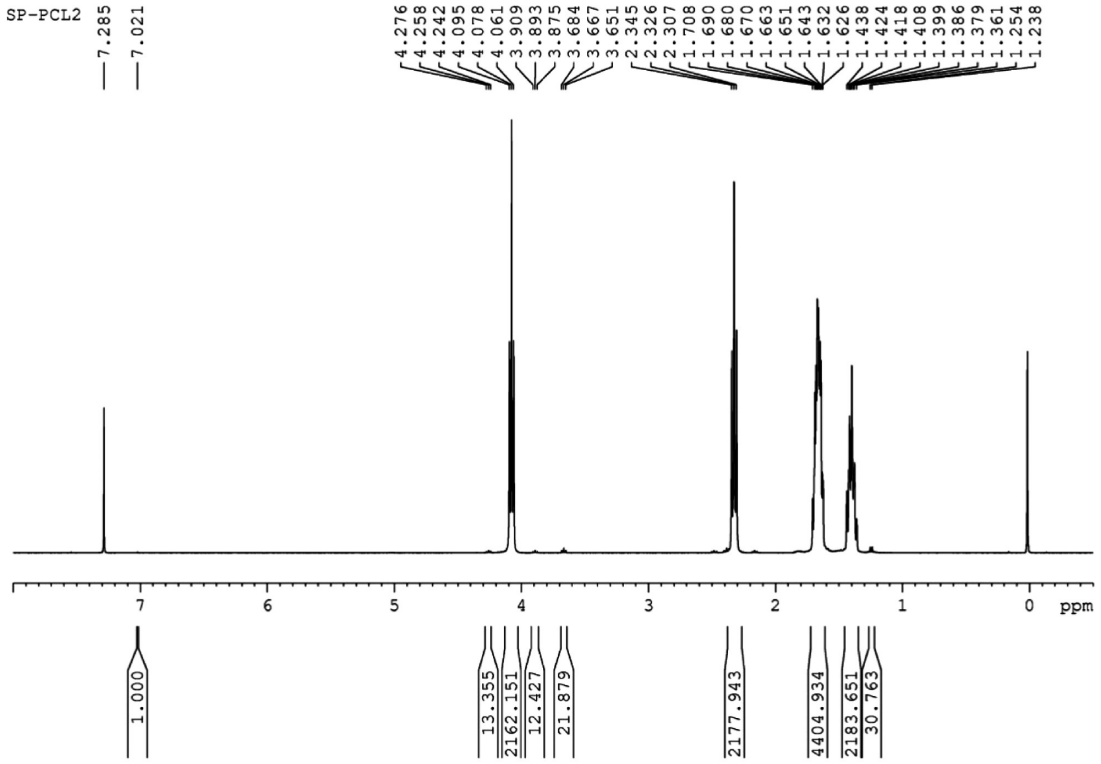

Figure 1. [1]H NMR spectrum of SP-PCL.

Scheme 2. Photochromic and Fluorescence Switching of SP-PCL Polymer Nanoparticles

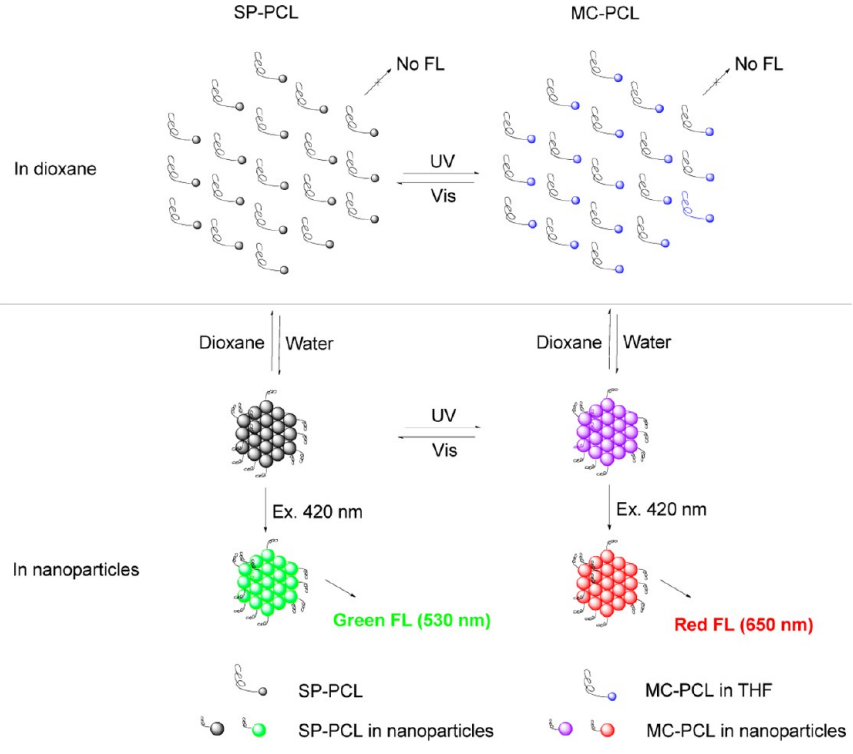

emission at 530 nm is clearly observed for SP-PCL nanoparticles (Figure 4). As shown in Figure 4a, the green emission intensity increases with water/dioxane volume ratio. The red emission intensity increases with water/dioxane volume ratio, too (Figure 4b). Therefore, both green and red emissions are solvent-dependent. Similar green emission has been reported for the donor-substituted SPs,[32] and our work further demonstrates that even without a donor-substituted group, SPs also emit green fluorescence in SP-conjugated PCL nanoparticle, which definitely deserves deep following investigation about the molecular photophysical mechanism in the future. Nevertheless, both the green and red emissions are found to be

dx.doi.org/10.1021/ma5001157 | *Macromolecules* XXXX, XXX, XXX−XXX

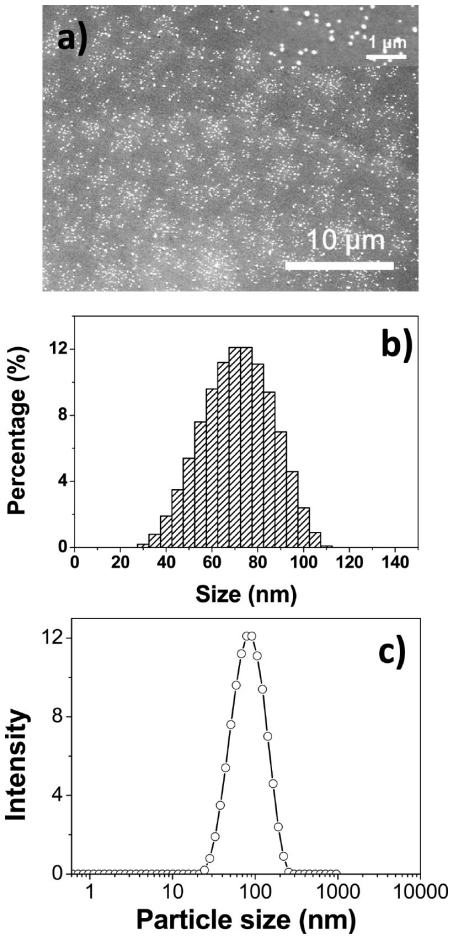

Figure 2. (a) SEM image of SP-PCL nanoparticles. (b) Size distribution of SP-PCL nanopartciles. (c) DLS profile of SP-PCL nanoparticles.

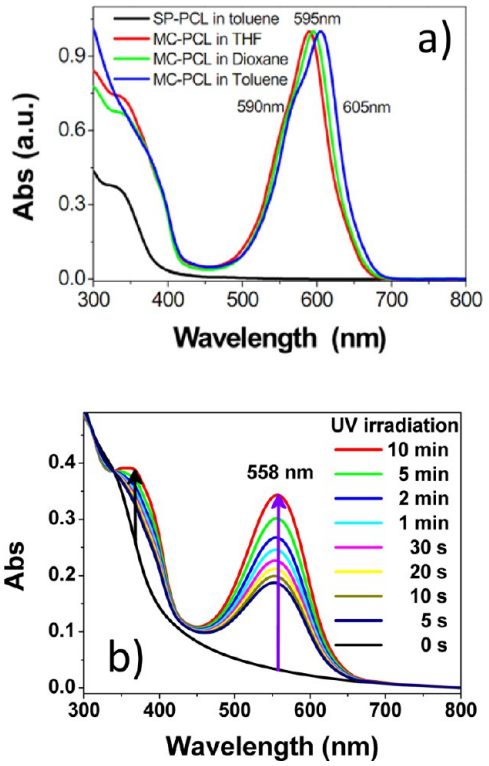

Figure 3. Photochromism. (a) Absorption spectra of SP-PCL in different solvents. (b) Time-dependent absorption spectra of SP-PCL nanoparticle dispersion in aqueous media under UV 365 nm irradiation.

significantly enhanced with increasing water/dioxane volume ratios likely owing to aggregation of SP-PCL chains or limitation of SP rotation inside the polymer nanoparticles, which is analogous to aggregation-induced emission enhancement extensively reported.[33−35]

The fluorescence spectra of photoswitchable SP-PCL nanoparticles under the excitation at different wavelengths disclose not only the photonic energies required for fluorescence excitation but also photoisomerization state of SPs. Generally, it is known that UV irradiation induces transformation of SP into MC form, while visible light illumination causes the inverse photoisomerization. However, the exact critical switching wavelength for SP-MC transformation has not been determined experimentally until excitation wavelength-dependent fluorescence spectra became available. The change of fluorescence spectra under continuous excitation at different wavelengths was then used for determination of critical switching wavelength (Figure 5). It is evident that SP emission intensity decreases and simultaneously MC emission intensity increases at continuous 410 nm excitation, indicating more SP groups are transformed to MC form inside nanoparticles (Figure 5a). On the other hand, continuous excitation with long-wavelength light at above 420 nm drives MC back to SP form (Figure 5c). Therefore, for the SP-PCL nanoparticles, regardless of the form of SP or MC, all the fluorescence spectra in the following study are recorded with the excitation wavelength at 420 nm, at which the photoinduced conversion rates of MC to SP and SP to MC are found to be equal (Figure 5b). Figure 5d shows the time-dependent change of green and red emission intensity at 530 and 650 nm upon different wavelength excitation. We conclude that 410 nm excitation results in obvious SP-MC transformation, whereas 430 nm excitation causes slight reverse photoisomerization from MC to SP. Therefore, we choose the critical wavelength at 420 nm as the excitation wavelength, which minimizes the photoinduced isomerization.

Figure 6 presents the dynamic change of fluorescence spectra of photoswitchable nanoparticles in water under 365 nm UV irradiation and the reverse process. The green emission from SP decreases at the beginning while red emission from MC increases upon 365 nm UV irradiation. Twenty seconds irradiation at 1.0 mW/cm^2 is required to attain the transformation equilibrium from SP to MC form in PCL nanoparticles (Figure 6a). The relatively slower switching speed than SP-PCL solution (normally less than 5 s) originates from the restricted molecule motion in the localized "sticky solid-like" microenvironment inside SP-PCL nanoparticles, where configuration switching must overcome the energetic barriers imposed by the closely coiled polymer chains. Although the switching speed is somewhat slow in SP-PCL nanoparticles, the reversibility of photoswitching is obviously improved as side reactions are suppressed due to decreased photobleaching in oxygen-shielded SP-PCL nanoparticles. Consequently, in the reverse process, the red emission at 650 nm from MC form disappears while the emission intensity at 530 nm from SP can be almost completely recovered to the original level after about 6 min under continuous 420 nm excitation (Figure 6b).

The reversible fluorescence switching of the SP-PCL nanoparticles is further highlighted with alternating UV (λ < 420 nm) and visible (λ > 420 nm) light irradiation. As shown in

dx.doi.org/10.1021/ma5001157 | Macromolecules XXXX, XXX, XXX−XXX

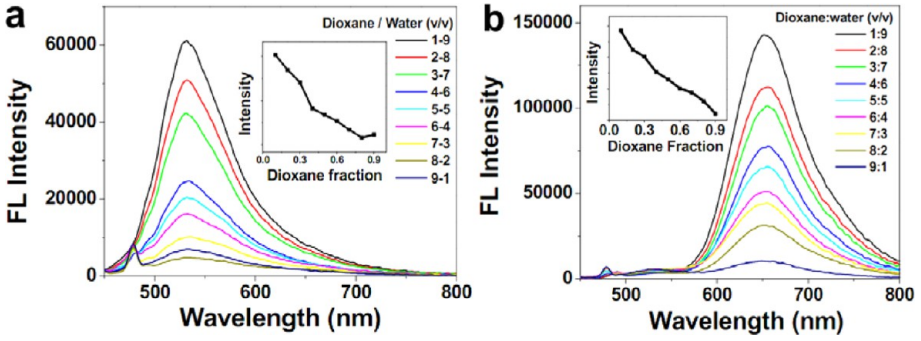

Figure 4. Fluorescence spectra of SP-PCL in dioxane/water with various volume ratios before (a) and after (b) 365 nm UV irradiation for 20 s. All excitation wavelengths are set at 420 nm.

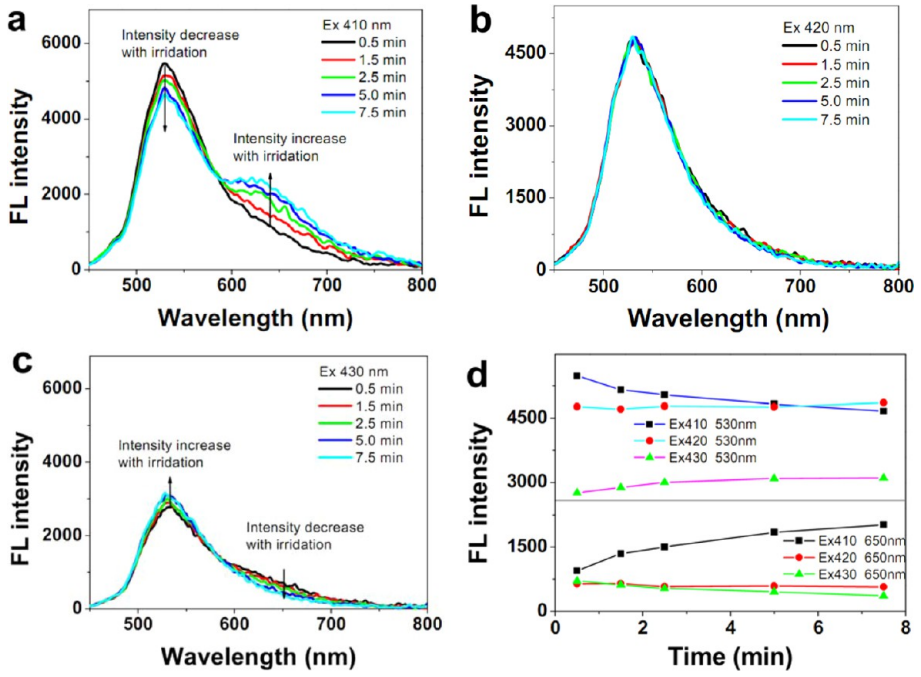

Figure 5. Change of fluorescence spectra under continuous excitation at different wavelengths: (a) 410, (b) 420, and (c) 430 nm. (d) Intensity versus scanning times.

Figure 6c, fluorescence switching of SP-PCL nanoparticles with UV and visible light is highly reversible without noticeable decay in fluorescent intensity at least for six cycles. The wavelength at which fluorescence at 650 nm is most rapidly switched on is about 300−400 nm, corresponding to the main absorption shoulder of SP form (black curve in Figure 3b). Similarly, irradiation at around 558 nm, which is the absorption band of MC form (red curve in Figure 3b), causes rapid quenching of fluorescence at 650 nm accompanied by simultaneous fluorescence increase at 530 nm. These irradiation energies are well resolved, therefore, affording clear separation between switching wavelength (300−400 and 558 nm) and fluorescence excitation wavelength (420 nm).

On the basis of the above spectrum survey, we propose the photochemical and photophysical processes of SP-PCL nanoparticles under irradiation/excitation at different wavelengths (Figure 6d). Obviously, the photochemical process is strongly coupled to the fluorescence process in our system. Irradiation with UV light at below 420 nm can induce both photoswitching and red fluorescence, while only green emission is observed under visible light irradiation at above 420 nm. This indicates that SPs in nanoparticles emit green fluorescence before they are transformed into MC form with red emission. Fluorescence switching of SPs, which is involved in radiation decays, is more complicated than general photochromic processes. In previous reports, no green emission was observed because in solution or nanoparticles, the nonradiative decay of excited SP* (internal conversion, IC) predominates over the radiation process, causing ignorable green emission.[12] Here strong green and red emissions are observed because of the aggregation state and the crystalline state of SP-PCL. The XRD and DSC results indicate that SP-PCL polymers are semicrystalline. XRD results show that there are three distinct peaks at 2θ of 21.3°, 22.0°, and 23.6° in both SP-PCL bulk sample and SP-PCL nanoparticles, which are assigned to the diffraction of (110), (111), and (200) lattice planes, respectively (Figure 7a,b). The crystalline degree of both SP-PCL polymers and nanoparticles is measured to be 80% and 65%, respectively (Figure S1). Therefore, thanks to the crystalline nature of PCL matrix, the internal motion of SPs inside the SP-PCL nanoparticles is dramatically decreased, leading to large inhibition of nonradiative relaxation mechanism (IC). Hence, the radiation

dx.doi.org/10.1021/ma5001157 | Macromolecules XXXX, XXX, XXX−XXX

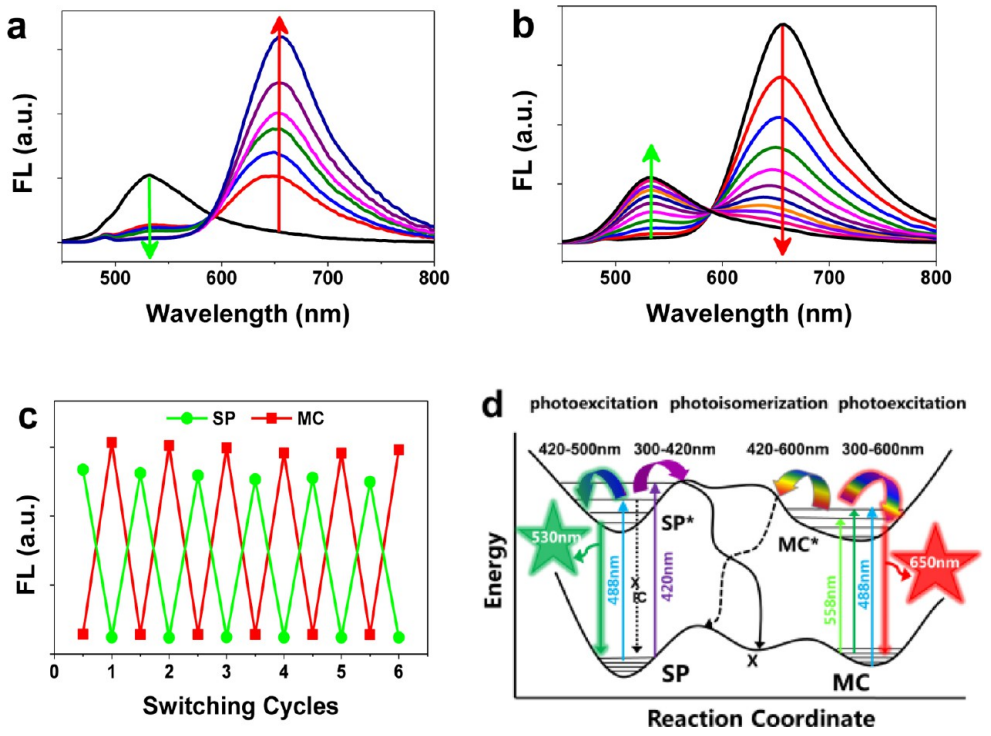

Figure 6. Fluorescence switching of SP-PCL nanoparticles. (a) Fluorescence spectra under exposure to 365 nm UV irradiation for 0, 2, 3, 5, 10, 15, and 20 s. (b) Time-dependent fluorescence spectra after 365 nm UV irradiation for 2 min. Excitation wavelength: 420 nm. Time: 24, 48, 72, 96, 120, 144, 168, 192, 216, 288, and 360 s. (c) Reversibility of fluorescence photoswitching of SP-PCL nanoparticles. The intensities of SP green emissions are multiplied by 3 for better contrast. (d) Diagram illustrating photochemical and photophysical processes of SP-PCL nanoparticles under different irradiation. SP* and MC* represent a vibrationally excited state of SP and MC, respectively. IC: internal conversion. Each wavelength represents a photochemical (photoisomerization) and/or photophysical (photoexcitation) process.

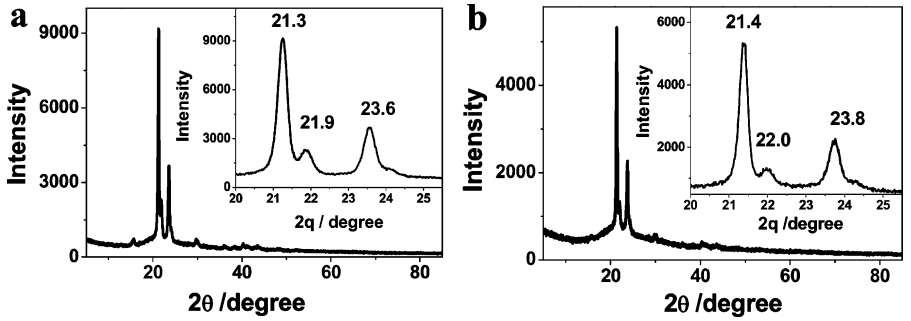

Figure 7. XRD patterns of SP-PCL nanoparticles. (a) SP-PCL sample was first dissolved in chloroform and then precipitated in dry ether. (b) SP-PCL sample was first dissolved in dioxane and then precipitated in water.

decay of SPs in SP-PCL nanoparticles under visible light becomes dominant, giving rise to the increased green fluorescence. The same reason causes the strong enhancement of red emission from MC in MC-PCL nanoparticles.

Photoswitchable Fluorescence Imaging. As a demo, a pattern constructed with SP-PCL nanoparticles shows tunable green and red fluorescent microscopic images under exposure to irradiation of different wavelengths, which could be repeated for at least tens of times, indicating the great reversibility of fluorescent switching (Figure 8). SP-PCL nanoparticles are biodegradable because the PCL macromolecules have been extensively used as drug delivery carriers for decades, which are eventually metabolized into carbon dioxide and water in living cell after accomplishing their mission for cellular imaging or sensing. We conducted the imaging experiments to examine the potential applications of biodegradable SP-PCL nanoparticles as bioimaging agents. Preliminary experimental results about liposome-mediated delivery of SP-PCL nanoparticles indicate that the SP-PCL nanoparticles are straightforwardly internalized into living cells (Figure 9). The results suggest that SP-PCL nanoparticles can be fused into membranes and internalized into cells and have no noticeable toxic effects on live cells. The SP-PCL nanoparticles in the cells produce green fluorescence at 473 nm excitation, while red fluorescence is obtained at 561 nm excitation after 405 nm laser activation for 1 s. The cellular imaging essays indicate that SP-PCL biodegradable polymer nanoparticles can be used as photoswitchable fluorophores for reversible bioimaging.

Super-Resolution Fluorescence Imaging. Super-resolution imaging based on the nanoscale localization of photoswitchable fluorophores has provided us unprecedented opportunity for observing many subcellular structures beyond the diffraction limit.[20,21] The photophysical and photochemical properties of fluorophores, in particular the photoswitching

dx.doi.org/10.1021/ma5001157 | *Macromolecules* XXXX, XXX, XXX−XXX

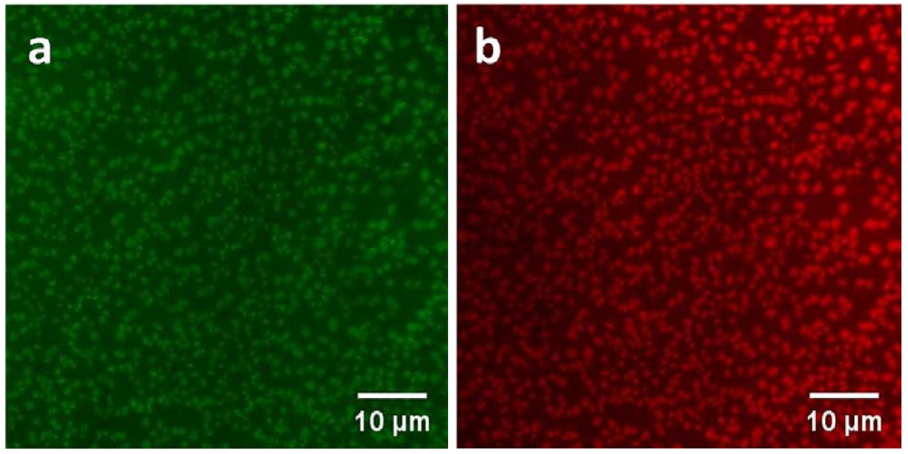

Figure 8. Fluorescence microscopy images of (a) SP-PCL nanoparticles at 473 nm laser excitation before 405 nm laser irradiation and (b) SP to MC transformation in nanoparticles at 561 nm laser excitation after 405 nm laser irradiation for 1 s.

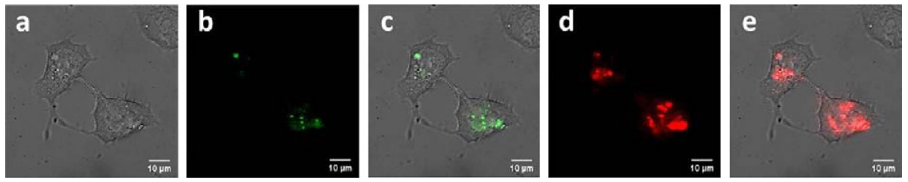

Figure 9. Reversible fluorescence tracing of SP-PCL nanoparticles in live cells. (a) Bright-field image displaying the position of cells. (b) SP-PCL nanoparticles at 473 nm excitation. (c) Merged image of SP-PCL nanoparticles in live cells. (d) MC-PCL nanoparticles at 561 nm excitation after 405 nm irradiation for 1 s. (e) Merged image of MC-PCL nanoparticles in live cells.

capability of fluorophores, are critical for localization-based super-resolution fluorescence imaging.[31,32] The on and off fluorescence of SP-PCL nanoparticles are found to be cycled under exposure to continuous 561 nm laser (2.0 kW/cm^2) and pulse 405 nm laser light (0.1 kW/cm^2) (Figure 9), which is understood that 561 nm light can only excite low-energy red emission at 650 nm rather than high-energy green emission at 530 nm. The responsive cycles are reversible and may be conducted at least ten times. Finally, we used SP-PCL nanoparticles in localization-based super-resolution microscopy for both subwavelength nanostructure and live cell imaging. First of all, to examine the imaging quality and resolution, we identified the nanolocalization of the embedded SP-PCL nanoparticles in the solid films by a home-built localization-based super-resolution microscopy (Figure 10). We continuously acquired 3000 frames at a frame rate of 15 Hz and detected about 9×10^4 nanoparticle switching events in total (Figure 10a). For each nanoparticle switching event, about 2700 photons were collected on average, corresponding to localization precision of 17 nm that is comparable to commonly used photoswitchable or activatable dyes (Figure 10b). Fluorescence of single SP-PCL nanoparticle can be turned on and off (Figure S2). A green laser (561 nm) excited fluorescence from MC form inside nanoparticles, and switched fluorescent MC form to dark SP form inside nanoparticles. A 405 nm laser recovered nonfluorescent SP form to fluorescent MC form inside nanoparticles. After 405 nm laser illumination, the fluorescence of single SP-PCL nanoparticle could be recovered immediately. Further comparison distinctly reveals that conventional fluorescent imaging is not competent to discriminate the vicinal SP-PCL nanoparticles (Figure 10c), but super-resolution imaging mode provided much clear images with sub-100 nm resolution (Figure 10d). Figures 10e and 10f exemplify the nearest distances between SP-PCL nanoparticles determined by the super-resolution images are 76 and 48 nm, respectively (Figures 10g and 10h). The results demonstrate that super-resolution imaging can surround the optical diffraction limitation, enabling two closed nanoparticles in sub-50 nm region well recognized in the super-resolution images.

SP-PCL nanoparticles were also cocultivated with Hela cells and observed by the same home-built localization-based super-resolution microscopy system followed by algorithm processing (Figure 11).[31,32] The bright-field image in Figure 11a displays that most of SP-PCL nanoparticles are nonspecifically attached to the cell because of the lipophilic nature of PCL chains. Evidently, in the regions where SP-PCL nanoparticles are too close, individual fluorescent nanoparticles cannot be clearly distinguished (Figure 11b,d). On the contrary, super-resolution images in Figure 11c,e,f showed clearly nanoscale localization of separated nanoparticles, each corresponding to an individual SP-PCL nanoparticle and resulting from repeated localizations of a single SP-PCL nanoparticle over multiple photoswitching cycles. For example, two SP-PCL nanoparticles of 50 nm apart became well differentiated in the super-resolution image (Figure 11f,g). The FWHM (full width at half-maximum) width and the $1/e^2$ diameter of the localized SP-PCL nanoparticles are determined from Gaussian fitting to be 27 ± 3 and 45 ± 5 nm, respectively. Importantly, this result demonstrates that super-resolution optical central localization is independent of the size of nanoparticles. The most recent research indicated that the average position precision of fluorescent molecular labels can even be below 1 nm regardless of the size of labels.[36] Thus, the super-resolution imaging method is capable of high localization precision down to 24 nm, which is comparable to that of scanning electron microscopy imaging of organic materials.

dx.doi.org/10.1021/ma5001157 | *Macromolecules* XXXX, XXX, XXX−XXX

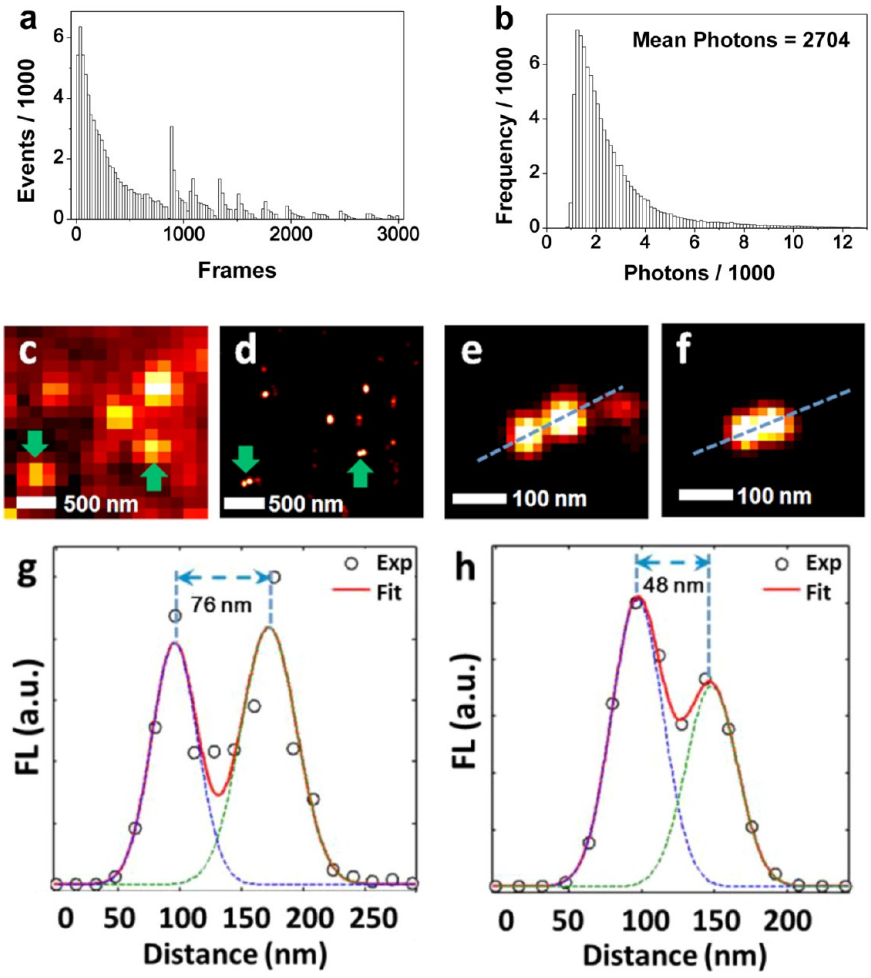

Figure 10. Super-resolution imaging of SP-PCL nanoparticles in poly(vinyl alcohol) (PVA) film. (a) Detected switching events vs acquired frames. (b) Distribution of photons per single nanoparticle. (c) Conventional fluorescent image displaying the distribution of SP-PCL nanoparticles in solid film. (d) Super-resolution fluorescent imaging for (c). (e) and (f) represent two pairs of vicinal SP-PCL nanoparticles in (d). (g) and (h) Fluorescence cross-sectional profiles of two pairs of vicinal SP-PCL nanoparticles along the dashed lines in (e) and (f).

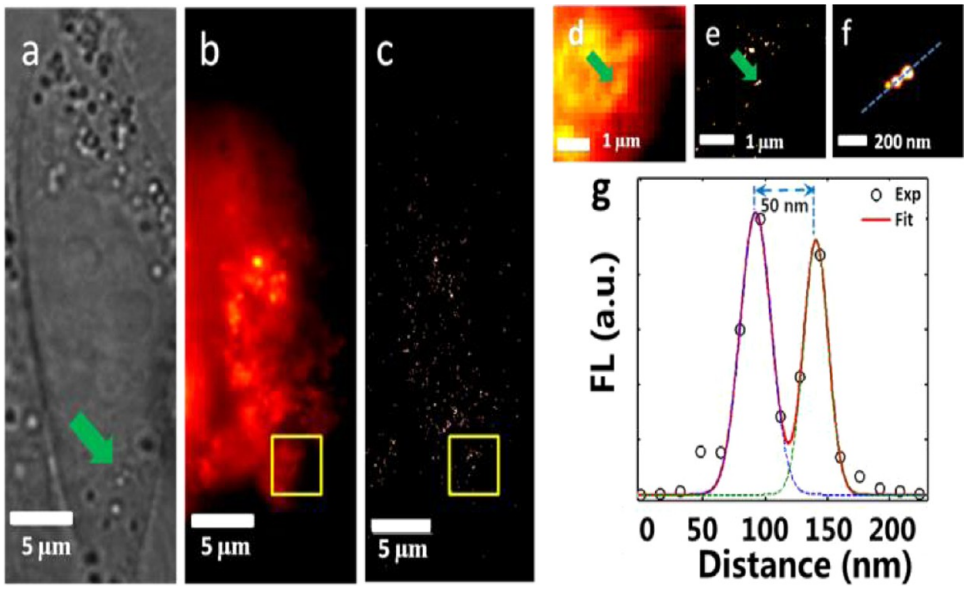

Figure 11. Super-resolution imaging of SP-PCL nanoparticles in live cells. (a) Bright-field image displaying the position of SP-PCL nanoparticles in the cell. (b) Conventional fluorescent image displaying the distribution of SP-PCL in live cells. (c) Super-resolution fluorescent imaging for (b). (d) A magnified view of the boxed region in (b). (e) A magnified super-resolution imaging of the marked region in (c), corresponding to (d). (f) A magnified view of the marked region in (e). (g) Fluorescence cross-sectional profile of two vicinal SP-PCL nanoparticles along the dashed lines in (f).

dx.doi.org/10.1021/ma5001157 | *Macromolecules* XXXX, XXX, XXX−XXX

In conclusion, we fabricated biodegradable SP-PCL nanoparticles capable of undergoing reversible fluorescence switching with alternating UV (<420 nm) and visible (>420 nm) light. The outstanding advantages of photoswitchable SP-PCL nanoparticles, e.g., fast response, good stability and robustness, and great biocompatibility and biodegradability, endow them to act as excellent fluorescent probes in super-resolution imaging. The localization-based super-resolution fluorescence imaging results demonstrate that vicinal SP-PCL nanoparticles are discernible with sub-50 nm resolution, which is much higher than that obtained with conventional fluorescent imaging. In addition to their promising application in bioimaging, we expect that such high signal-to-noise, environmentally friendly, and fluorescence-switchable nanomaterials will exhibit potential utility in many fields like smart inks and photosensitive displays.

■ ASSOCIATED CONTENT

Ⓢ Supporting Information

Methods and characterization data. This material is available free of charge via the Internet at http://pubs.acs.org.

■ AUTHOR INFORMATION

Corresponding Authors

*E-mail: mqzhu@hust.edu.cn (M.-Q.Z.).
*E-mail: leo@mail.hust.edu.cn (Z.-L.H.).
*E-mail: sliu@ustc.edu.cn (S.L.).

Author Contributions

§G.-F.Z. and Z.H. contributed equally to this work.

Notes

The authors declare no competing financial interest.

■ ACKNOWLEDGMENTS

This work was supported by the National Science Foundation of China (NSFC 21174045, 30970691, 30925013, and 51033005) and National Basic Research Program of China (2013CB922104, 2011CB910401). M.P.A. is the Foreign Young Investigator Awardee of NSFC (21150110141 and 21250110572). We also gratefully thank the support from the Analysis Center in Huazhong University of Science and Technology.

■ REFERENCES

(1) Berkovic, G.; Krongauz, V.; Weiss, V. *Chem. Rev.* **2000**, *100*, 1741−1754.
(2) (a) Fomina, N.; Sankaranarayanan, J.; Almutairi, A. *Adv. Drug Delivery Rev.* **2012**, *64*, 1005−1020. (b) Gohy, J. F.; Zhao, Y. *Chem. Soc. Rev.* **2013**, *42*, 7117−7129. (c) Habault, D.; Zhang, H.; Zhao, Y. *Chem. Soc. Rev.* **2013**, *42*, 7244−7256. (d) Jochum, F. D.; Theato, P. *Chem. Soc. Rev.* **2013**, *42*, 7468−7483. (e) Zhao, Y. *J. Mater. Chem.* **2009**, *19*, 4887. (f) Zhao, Y. *Macromolecules* **2012**, *45*, 3647−3657.
(3) (a) Achilleos, D. S.; Hatton, T. A.; Vamvakaki, M. *J. Am. Chem. Soc.* **2012**, *134*, 5726−5729. (b) Pasparakis, G.; Vamvakaki, M. *Polym. Chem.* **2011**, *2*, 1234−1248.
(4) Irie, M. *Chem. Rev.* **2000**, *100*, 1685−1716.
(5) Irie, M.; Fukaminato, T.; Sasaki, T.; Tamai, N.; Kawai, T. *Nature* **2002**, *420*, 759−760.
(6) Feringa, B. L, Ed.; *Molecular Switches*; Wiley-VCH: Weinheim, 2001.
(7) Shao, N.; Jin, J. Y.; Wang, H.; Zheng, J.; Yang, R. H.; Chan, W. H.; Abliz, Z. *J. Am. Chem. Soc.* **2010**, *132*, 725−736.
(8) (a) Minkin, V. I. *Chem. Rev.* **2004**, *104*, 2751−2776. (b) Li, C. H.; Zhang, Y. X.; Hu, J. M.; Cheng, J. J.; Liu, S. Y. *Angew. Chem., Int. Ed.* **2010**, *49*, 5120−5124. (c) Wu, T.; Zou, G.; Hu, J. M.; Liu, S. Y. *Chem. Mater.* **2009**, *21*, 3788−3798.
(9) Chen, Q.; Feng, Y.; Zhang, D.; Zhang, G.; Fan, Q.; Sun, S.; Zhu, D. *Adv. Funct. Mater.* **2010**, *20*, 36−42.
(10) Grzelczak, M.; Vermant, J.; Furst, E. M.; Liz-Marzan, L. M. *ACS Nano* **2010**, *4*, 3591−3605.
(11) Zhu, M.-Q.; Zhu, L.; Han, J. J.; Wu, W.; Hurst, J. K.; Li, A. D. Q. *J. Am. Chem. Soc.* **2006**, *128*, 4303−4309.
(12) Zhu, M. Q.; Zhang, G. F.; Li, C.; Aldred, M. P.; Chang, E.; Drezek, R. A.; Li, A. D. Q. *J. Am. Chem. Soc.* **2011**, *133*, 365−372.
(13) (a) Zhu, M. Q.; Zhang, G. F.; Li, C.; Li, Y.-J.; Aldred, M. P.; Li, A. D. Q. *J. Innov. Opt. Health Sci.* **2011**, *4*, 395−408. (b) Li, C. H.; Liu, S. Y. *Chem. Commun.* **2012**, *48*, 3262−3278.
(14) Hell, S. W.; Wichmann, J. *Opt. Lett.* **1994**, *19*, 780−782.
(15) Betzig, E.; Patterson, G. H.; Sougrat, R. O.; Lindwasser, W.; Olenych, S.; Bonifacino, J. S.; Davidson, M. W.; Lippincott-Schwartz, J.; Hess, H. F. *Science* **2006**, *313*, 1642−1645.
(16) Gustafsson, M. G. L. *Proc. Natl. Acad. Sci. U. S. A.* **2005**, *102*, 13081−13086.
(17) Rust, M. J.; Bates, M.; Zhuang, X. *Nat. Methods* **2006**, *3*, 793−795.
(18) Betzig, E.; Patterson, G. H.; Sougrat, R.; Lindwasser, O. W.; Olenych, S.; Bonifacino, J. S.; Davidson, M. W.; Lippincott-Schwartz, J.; Hess, H. F. *Science* **2006**, *313*, 1642−1645.
(19) Hell, S. W. *Science* **2007**, *316*, 1153−1158.
(20) Huang, B.; Wang, W.; Bates, M.; Zhuang, X. *Science* **2008**, *319*, 810−813.
(21) Huang, B.; Jones, S. A.; Brandenburg, B.; Zhuang, X. *Nat. Methods* **2008**, *5*, 1047−1052.
(22) Dempsey, G. T.; Vaughan, J. C.; Chen, K. H.; Bates, M.; Zhuang, X. *Nat. Methods* **2011**, *8*, 1027−1036.
(23) Bates, M.; Huang, B.; Dempsey, G. T.; Zhuang, X. *Science* **2007**, *317*, 1749−1753.
(24) Fölling, J.; Belov, V.; Kunetsky, R.; Medda, R.; Schönle, A.; Egner, A.; Eggeling, C.; Bossi, M.; Hell, S. W. *Angew. Chem., Int. Ed.* **2007**, *46*, 6266−70.
(25) (a) Yildiz, I.; Impellizzeri, S.; Deniz, E.; McCaughan, B.; Callan, J. F.; Raymo, F. M. *J. Am. Chem. Soc.* **2011**, *133*, 871−879. (b) Gu, H.; Bi, L.; Fu, Y.; Wang, N.; Liu, S.; Tang, Z. *Chem. Sci.* **2013**, *4*, 4371−4377. (c) Liu, Z.; Tang, Z. *Nano Today* **2010**, *5*, 267−281. (d) Qin, B.; Chen, H.; Liang, H.; Fu, L.; Liu, X.; Qiu, X.; Liu, S.; Song, R.; Tang, Z. *J. Am. Chem. Soc.* **2010**, *132*, 2886−2888.
(26) Ercole, F.; Davis, T. P.; Evans, R. A. *Polym. Chem.* **2010**, *1*, 37−54.
(27) Raymo, F. M.; Giordani, S. *J. Am. Chem. Soc.* **2001**, *123* (19), 4651−4652.
(28) Fan, J.-B.; Yang, K.; Yi, H.-Q.; Fu, T.; Xia, M.-X.; Xu, X.-B.; Zhu, M.-Q. *Chem. Commun.* **2010**, *46*, 5805−5807.
(29) Fan, J.-B.; Long, F.; Aldred, M. P.; Li, Y.-J.; Liang, Z.-W.; Zhu, M.-Q. *Macromol. Chem. Phys.* **2012**, *213*, 1499−1508.
(30) Quan, T. W.; Li, P. C.; Long, F.; Zeng, S. Q.; Luo, Q. M.; Hedde, P. N.; Nienhaus, G. U.; Huang, Z. L. *Opt. Express* **2010**, *18*, 11867−11876.
(31) Quan, T. W.; Zeng, S. Q.; Huang, Z. L. *J. Biomed. Opt.* **2010**, *15*, 066005.
(32) Tian, Z.; Wu, W.; Wan, W.; Li, A. D. Q. *J. Am. Chem. Soc.* **2009**, *131*, 4245−4252.
(33) Aldred, M. P.; Li, C.; Zhang, G.-F.; Gong, W.-L.; Zhu, M.-Q. *J. Mater. Chem.* **2012**, *22*, 7515−7528.
(34) Zhang, G.-F.; Aldred, M. P.; Gong, W.-L.; Li, C.; Zhu, M.-Q. *Chem. Commun.* **2012**, *48*, 7711−7713.
(35) Aldred, M. P.; Li, C.; Zhu, M.-Q. *Chem.—Eur. J.* **2012**, *18*, 16037−16045.
(36) Szymborska, A.; Marco, A.; Daigle, N.; Cordes, V. C.; Briggs, J. A. G.; Ellenberg, J. *Science* **2013**, *341*, 655−658.